IUST
Iran University of Science and Technology

Iranian Journal of Electrical and Electronic Engineering

Journal Homepage: ijeee.iust.ac.ir

A Mechanically Coupled Magnetic Geared Machine: Semi-Analytical, Numerical and Experimental Study on Performance Characteristics

A. Jabbari*(C.A.), H. Moradzadeh**, and R. Lotfi***.

Abstract: Along with the development of hybrid electric vehicles, researchers are trying to reduce existing limitations such as noise and environmental concerns and improve the efficiency and reliability of these systems. The use of magnetic gear technology is one of the solutions that have been recently proposed to remove these limitations and achieve higher benefits. In this paper, a mechanically coupled magnetic geared (MCMG) machine has been introduced. An accurate analytical model based on the subdomain method is presented to calculate the magnetic machine performance. To do this, first, a pseudo-Cartesian coordinate system is specified, and then the constitutive equations, i.e. Laplace's and Poisson's equations are rewritten for different regions of the machine. The separation of variables method was used to determine the general solution of the equations. Then by applying appropriate interface and boundary conditions, the Fourier coefficients of the equations were determined. To verify the analytical results, the performance of the proposed magnetic machine is numerically simulated using the finite element method in commercial software, and then a prototype is built and tested in three distinct modes. By comparing the analysis results with numerical simulation results and experimental tests, the high accuracy of the proposed analytical model can be confirmed.

Keywords: Mechanically Coupled Magnetic Gear, Subdomain Method, Finite Element Method, Prototyping, Hybrid Electric Vehicle.

1 Introduction

CURRENTLY, with the development of permanent magnet machines including magnetic gears with rare earth materials, the torque characteristics and efficiency of these machines have been significantly improved [1-3]. Typically, in applications such as hybrid electric vehicles, a mechanical power transmission system is used to achieve high torque and low-speed [8]. Mechanical systems often require precise lubrication and maintenance and have limitations such as high vibration and noise, short life, etc. Machines called magnetic gears have now been invented which, unlike their mechanical counterparts, are non-contact and have high torque [7]. The working principle of this machine is based on the modulation of the magnetic flux in the magnetic transmission, and it can be considered a combination of a magnetic rotor and an electric motor/generator. With the non-contact power transmission system of this device, the dimensions of the device are greatly reduced and you can use its direct drive low-speed applications.

A review of the history and development of magnetic gear technologies in recent years is given in [8]. The aim of this work is to give readers some insight into the advantages and disadvantages,

Iranian Journal of Electrical & Electronic Engineering, 2023.
Paper first received 27 May 2023 and accepted 10 Dec 2023.
* The author is with Department of Manufacturing and Production Engineering, Faculty of Engineering, Arak University, Arak, 38156-8- 8849, Iran.
E-mail: a-jabbari@araku.ac.ir.
** The author is with Department of Electrical Engineering, Faculty of Engineering, Arak University, Arak, 38156-8- 8849, Iran.
E-mail: h-moradzadeh@araku.ac.ir.
*** The author is with Department of Mechanical Engineering, Faculty of Engineering, Arak University, Arak, 38156-8- 8849, Iran.
E-mail: rasullotfi87@gmail.com.
Corresponding Author: A. Jabbari.

challenges, opportunities, and technology readiness. In [9], the design and performance of a magnetic gear, which employs rare-earth magnets were described. Simulation studies have shown to have a transmitted torque density exceeding 100 kNm/m/sup 3/. The structure and the performance characteristics of a magnetic gear using SmCo 5 for the permanent magnet were studied in [10]. The magnetic gear has a gear ratio of 1/3 and the maximum transmitted torque is 5.5 Nm at the driven magnetic gear. The results of this study seem to be useful for the development of industrial application of noncontact magnetic gears. A summary of the state of the art in magnetic gear technology was presented in [11] and then investigated its potential for marine energy applications. A brief overview is given of the state of the marine energy industry and the environment in which marine energy converters (MECs) operate. A short history of MG development over the past century is then presented followed by a discussion of the leading MG technologies and their relative advantages. The design of a prototype concentric-type magnetic gear is evaluated in [12]. The effects that the mechanical bridges connecting the modulator segments have on the performance of the gear have been analyzed by using detailed two-dimensional (2D) finite element (FE) analysis. New ripple factors, which better correlate with torque ripple than the cogging factor are introduced in [13], and illustrate why designs with no integer gear ratios tend to have much smaller torque ripples than designs with integer gear ratios. Thus, it is recommended to select pole counts that result in an even number of modulators but not an integer gear ratio. A coaxial magnetic gear that offers higher torque density, lower cogging torque, and lower iron losses than its counterparts was proposed in [14]. The key is to newly employ a Halbach permanent-magnet (PM) array to constitute the PM poles in the inner rotor and a partial Halbach array for the outer rotor. The corresponding magnetic field distributions, torque transmission, and torque ripples are analytically discussed. The main aim of the work presented in [15] is the imposition of constraints for the multi-objective optimizations of magnetic gears. In order to reduce the computational effort, a semi-analytic design procedure is adopted, providing a fast simulation tool that can be embedded within an optimization loop. Magnetic, thermal, and mechanical constraints are discussed and embedded into a stochastic algorithm, in order to identify immediately infeasible geometries. To obtain a sinusoidal distribution of air gap magnetic field, in presented work in [16], an exact 2-D analytical method is proposed to calculate the magnetic field distribution in a concentric magnetic gear with Halbach permanent-magnet arrays, and analyze the relationship between the parameters and maximum static torque, the parameters include width of modulating ring core, height of modulating ring and thickness of outer rotor yoke.

Due to the greater number of mechanical parts, mechanically coupled magnetic geared machines have a higher degree of freedom compared to electric machines [17-19]. The ability to achieve continuous gear ratios in these machines increases the likelihood of using them in hybrid electric vehicles.

Nowadays, commercial software based on finite element analysis methods is used as a powerful tool for accurate performance analysis of permanent magnet motors/generators. Even in some of them, parametric modeling of the motor/generator is embedded. Despite this, the research results show that these capabilities are not generalized for the parametric modeling of the magnetic gearbox, and often the numerical modeling of these machines in commercial software is difficult and time-consuming.

By using the analytical technique based on the subdomain method, parametric modeling and accurate and fast estimation of the magnetic characteristics of magnetic gears are provided. In this method, after dividing the magnetic machine into several separate regions, partial differential equations are written for each region. In order to solve the equations, the method of separation of variables is used and the coefficients of the equations are obtained by considering the conditions of the junction of the adjacent regions.

Several works [21-41] have been reported in the field of analytical modeling of permanent magnet electric machines and the effect of parameters such as stator slots, magnetization direction [21, 22], permanent magnet arrangement [20,] [23] and magnetic permeability have been reviewed.

In limited works, including [24] and [25], simple analytical models for basic magnetic gears have been presented. Although these models are not sufficient for analytical modeling of mechanically geared machines, they can be used as a basis for accurate modeling of these machines in our research.

In this research, the design of an MCMG machine is presented, and then an analytical model based on the subdomain method is developed to accurately calculate the magnetic characteristics of the machine. In this model, several features such as magnetization orientation, slots, and permanent magnets topologies are taken into account.

To validate the results of the presented analytical model, a prototype has been designed, built and tested, and the results of the analytical modeling have been compared with the results of the experimental tests and numerical simulation. The evaluation of

these results shows that the maximum error percentage is less than 3%.

2 Model Construction

The components of the MCMG machine are introduced and an analytical model is presented to calculate its performance in different working modes.

2.1 Mechanically Geared Magnetic Machine

Typically, the powertrain is coupled to an electric motor to provide the desired speed/torque specifications. In the design of the proposed MCMG machine, the axis of the electric machine and the magnetic gearbox are common. In other words, the magnetic gearbox is built into the electric machine as an integrated system.

The components of this system include the high-speed PM rotor/low-speed PM rotor (common between the gearbox and the electric machine), and the modulator ring, which determine their performance status in different working modes including motor mode, and battery charging mode. For example, in battery charging mode, high-speed to low-speed transmission is performed by the MCMG machine. In motor mode, usually the high-speed rotor is common between the gearbox and the machine and is driven by the armature field. Different gear ratios can be achieved by keeping one of the gearbox components (i.e. permanent magnet rotor or ferromagnetic modulator) fixed.

Mechanically coupled machines have high torque density and are used for special applications such as electric vehicles. In addition, due to the CVT capability due to three rotors with rotational degrees of freedom, these machines are of great importance.

In Fig. 1, the schematic representation of the studied mechanically geared machine is given. Permanent magnets are mounted on the surface of the high-speed and low-speed rotors and a number of coils are wrapped around the stator teeth. By adjusting the rotational speed of a distinct component, the other two components rotate with a specific gear ratio. In other words, by fixing one part of the machine and moving its other two parts, the corresponding gear ratio of the driving parts is obtained.

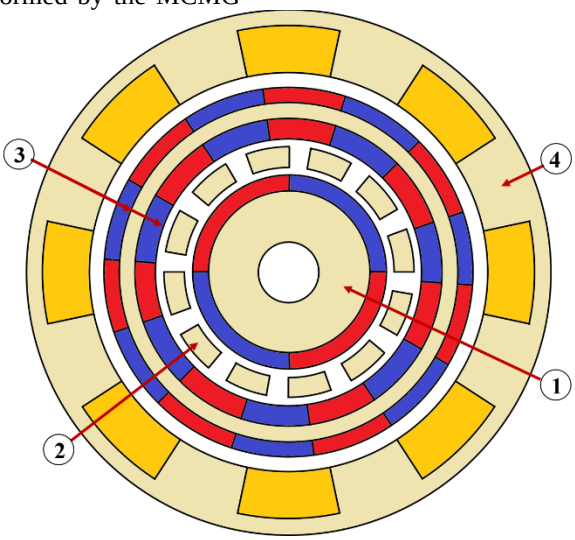

Fig. 1 A schematic of mechanically coupled magnetic geared machine. 1- Inner rotor, 2- modulator, 3- common rotor, 4- stator core.

In a magnetic gear, the following mathematical relationship is used to determine the number of ferromagnetic modulator parts [4]

$$N_m = p_i + p_o \tag{1}$$

where, p_i and p_o are the number of inner and outer rotor poles, respectively.
The relationship between the product of the number of parts and their corresponding rotational speed is calculated from the following formula

$$N_m\Omega_m = p_i\Omega_i + p_o\Omega_o \tag{2}$$

where Ω is the mechanical angular velocity of the respected components.
Considering the conservation of energy law as well as the gear effect [12] or field modulation [23], the torque relation can be expressed as follows

$$T_i + T_m + T_o = 0 \tag{3}$$

$$T_i\Omega_i + T_m\Omega_m + T_o\Omega_o = 0 \tag{4}$$

where, T_i, T_m and T_o are the inner rotor, modulator, and outer rotor torque, respectively.

In low-speed/high-torque mode, the inner rotor is connected to the driver and the outer rotor/ modulator is connected to the load. In this case, the modulation effect is calculated by the gear index as follow

$$G_r = \frac{T_o}{T_i} = -\frac{\Omega_i}{\Omega_o} = \frac{p_o}{p_i} \quad \text{or} \quad G_r = \frac{T_m}{T_i} = \frac{\Omega_i}{\Omega_m} = \frac{N_m}{p_i} \tag{5}$$

In this research, the modulator consists of 14 ferromagnetic parts and the internal and external rotors consist of 2 and 12 pairs of poles, respectively.

2.1.1. Subdomain Method Implementation

In the subdomain method, the machine geometry is divided into several distinct regions. Then Laplace's equation (for airgap and ferromagnetic regions) or Poisson's equation (for windings and magnet regions) are written. Then, appropriate boundary and interface conditions are applied and the general solution of the equations is determined by the method of separation of variables. Finally, by using the method of Fourier series, the coefficients of the equations are determined. Now, by solving a set of equations, it is possible to estimate the values of flux and torque in different areas of the machine.

The magnetic vector potential in air gap and ferromagnetic regions can be expressed according to Laplace's equation in polar system as follow

$$\frac{\partial^2 A(r.\theta)}{\partial r^2} + \frac{1}{r}\frac{\partial A(r.\theta)}{\partial r} + \frac{1}{r^2}\frac{\partial^2 A(r.\theta)}{\partial \theta^2} = 0 \quad \text{for} \begin{cases} R_1 \le r \le R_2 \\ \theta_1 \le \theta \le \theta_2 \end{cases} \tag{6}$$

The magnetic vector potential for the permanent magnet and coil areas can be calculated from Poisson's equation in the polar system according to the following equation

$$\frac{\partial^2 A(r.\theta)}{\partial r^2} + \frac{1}{r}\frac{\partial A(r.\theta)}{\partial r} + \frac{1}{r^2}\frac{\partial^2 A(r.\theta)}{\partial \theta^2} = f(r.\theta) \quad \text{for} \begin{cases} R_1 \le r \le R_2 \\ \theta_1 \le \theta \le \theta_2 \end{cases} \tag{7}$$

The results of previous work [23] shows that simpler mathematical models for magnetic gearboxes can be achieved by defining the pseudo-Cartesian coordinate system and rewriting the Laplace's and Poisson's equations in the new system. Fig. 2 shows the two-dimensional geometric model of the studied MCMG machine in polar and pseudo-Cartesian coordinate systems. The Laplace's and Poisson's equations in the new system are

$$\frac{\partial^2 A}{\partial t^2} + \frac{\partial^2 A}{\partial \theta^2} = 0 \quad \text{for} \begin{cases} t_1 \le t \le t_2 \\ \theta_1 \le \theta \le \theta_2 \end{cases} \tag{8}$$

$$\frac{\partial^2 A}{\partial t^2} + \frac{\partial^2 A}{\partial \theta^2} = f(t.\theta) \quad \text{for} \begin{cases} t_1 \le t \le t_2 \\ \theta_1 \le \theta \le \theta_2 \end{cases} \tag{9}$$

where $t = ln(\frac{r}{R_1})$, $t_1 = ln\left(\frac{R_2}{R_1}\right)$ and $t_2 = 0$.

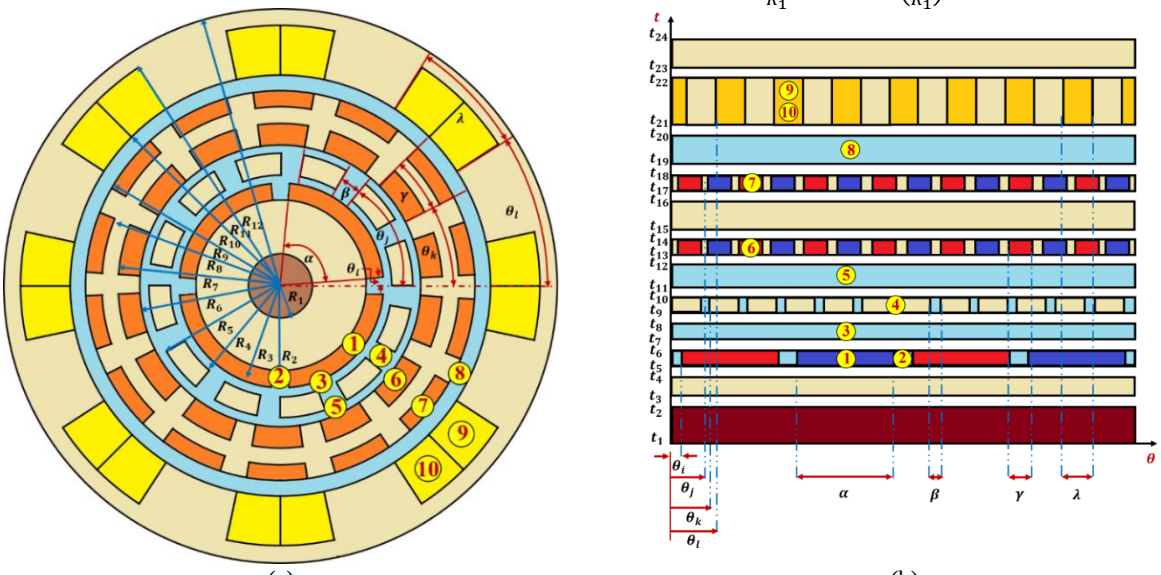

(a) (b)

Fig. 2 The MCMG machine geometry in (a) polar and (b) quasi-Cartesian coordinate system.

The magnetic vector potential for periodic regions is calculated from equation (10). If the region is non-periodic, the magnetic vector potential can be calculated from (11) [23].

$$A_{z\Omega}(t.\theta) = {a_0}^{\Omega} + {b_0}^{\Omega}t - f_{z\Omega}(t) + \sum_{n=1}^{\infty}\frac{1}{n}\left({a_n}^{\Omega}\frac{Sh\big(n(t-t_2)\big)}{Sh\big(n(t_1-t_2)\big)} + {b_n}^{\Omega}\frac{Sh\big(n(t-t_1)\big)}{Sh\big(n(t_2-t_1)\big)}\right)Cos(n\theta) + \sum_{n=1}^{\infty}\frac{1}{n}\left({c_n}^{\Omega}\frac{Sh\big(n(t-t_2)\big)}{Sh\big(n(t_1-t_2)\big)} + {d_n}^{\Omega}\frac{Sh\big(n(t-t_1)\big)}{Sh\big(n(t_2-t_1)\big)}\right)Sin(n\theta) \quad (10)$$

$$A_{z\Omega(j)}(t.\theta) = {a_0}^{\Omega(j)} + {b_0}^{\Omega(j)}t - f_{z\Omega(j)}(t) + \sum_{h=1}^{\infty}\left(\frac{{a_h}^{\Omega(j)}}{\nu_{h.\Omega(j)}}\frac{Ch\big(\nu_{h.\Omega(j)}(t-t_2)\big)}{Sh\big(\nu_{h.\Omega(j)}(t_1-t_2)\big)} + \frac{{b_h}^{\Omega(j)}}{\nu_{h.\Omega(j)}}\frac{Ch\big(\nu_{h.\Omega(j)}(t-t_1)\big)}{Sh\big(\nu_{h.\Omega(j)}(t_2-t_1)\big)}\right)Cos\big(\nu_{h.\Omega(j)}(\theta-\theta_1)\big) \quad (11)$$

In Fig. 3, comprehensive information about the characteristics of each region including the relevant equation, boundary and interface conditions of the studied MCMG machine is given. The general solutions of the equations for different areas are given in Table A1 to A5. The equations listed in Table A6 can be used to determine the coefficients of the equations in Tables A1 to A5 by using the Fourier series.

The radial and tangential flux density components are obtained for each sub-domain in polar coordination by using curl from the magnetic vector potential, i.e. $\boldsymbol{B} = \boldsymbol{\nabla} \times \mathrm{A}$ and the magnetic field intensity is calculated by (12) that for PM domains M is not zero and for the other domains $M = 0$.

$$H = \frac{B}{\mu_0\mu_r} - \frac{M}{\mu_r}$$

The torque is obtained using the Maxwell stress tensor and expressed as

$$T_e = \frac{L_s}{\mu_0}\int_0^{2\pi} BI_r(t_e.\theta).BI_\theta(t_e.\theta).d\theta \quad (13)$$

where $L_s$is the axial length of the machine and t_e is calculated by

$$t_e = ln\left(\frac{R_2}{R_e}\right) \text{ where } R_e = (R_2 + R_3)/2$$

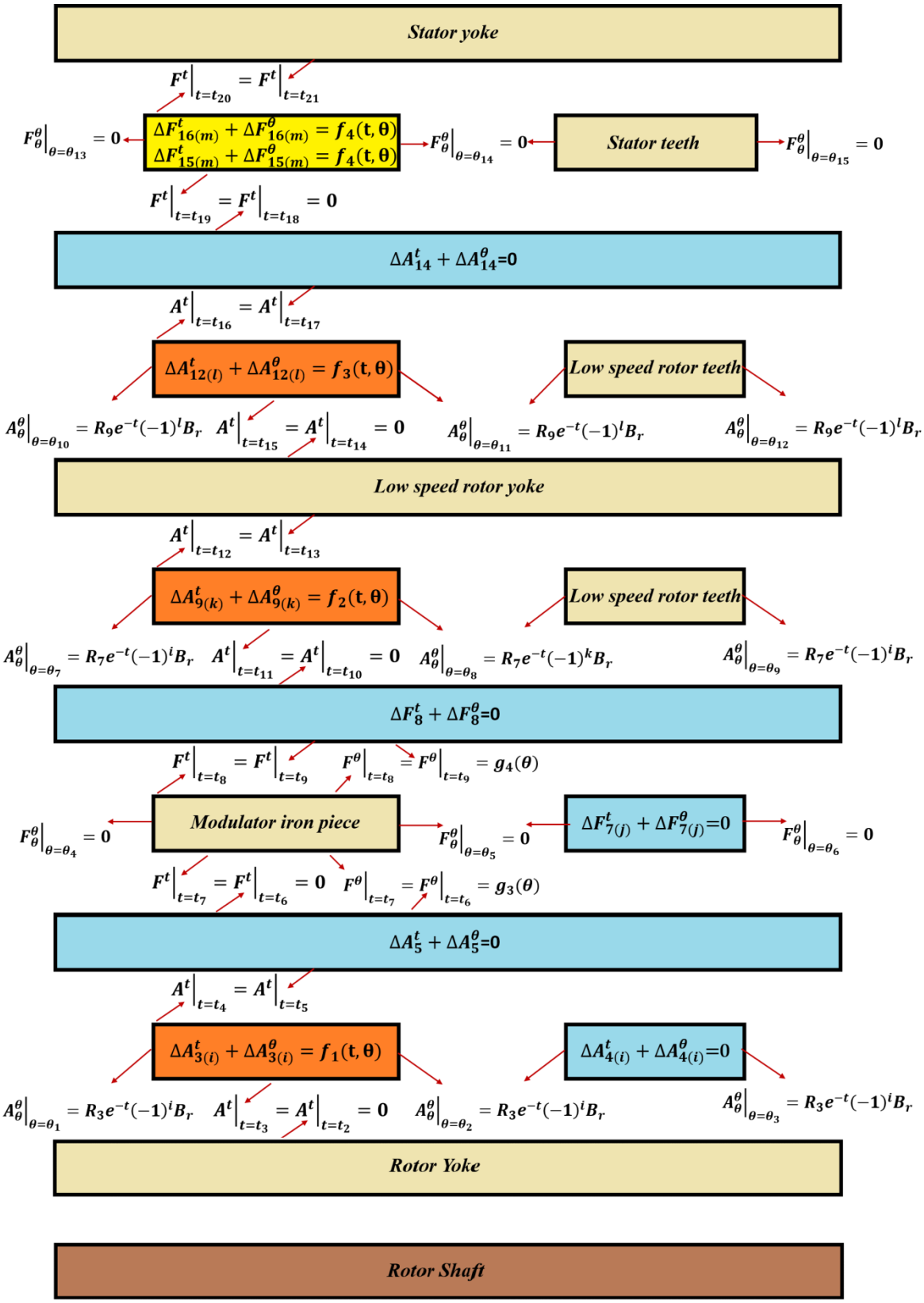

Fig. 3 Comprehensive information of equations and corresponding boundary conditions of each MCMG machine region.

3 Analytical Model Verification

In addition to the analytical modeling of the introduced machine, numerical simulation has been done in the finite element software and a machine prototype has been fabricated. The analytical modeling results have been compared with the results of numerical simulation and experimental tests in three working modes. Tables 1 and 2 list the dimensional and magnetic characteristics of the studied machine, respectively. Fig. 4 and 5 show the distribution of magnetic vector potential and magnetic flux density in the MCMG machine, respectively. The performance results of the machine in three working modes have been compared analytically and numerically. In this study the length of first, second and third airgaps are 0.5, 0.5 and 1.25 mm, respectively. The induced voltage values of the proposed machine in two modes of low-speed and high speed are obtained, respectively 8.74 and 12.42 volts. The power of the system is calculated to be about 31 watts for a speed of 300 rpm and a torque of 2 Nm.

Table 1 Dimensional features of the studied MCMG machine.

Symbol	Value	Symbol	Value	Symbol	Value
R_1	5.5	θ_1	36	θ_{13}	5
R_2	33	θ_2	72	θ_{14}	10
R_3	35	θ_3	108	θ_{15}	15
R_4	35.5	θ_4	11	θ_j	18
R_5	40	θ_5	22	α	36
R_6	40.5	θ_6	33	θ_k	16.5
R_7	42.5	θ_7	1	β	11
R_8	48.5	θ_8	15	θ_h	22.5
R_9	50.5	θ_9	29	δ	15
R_{10}	52	θ_{10}	4	θ_i	7.5
R_{11}	63	θ_{11}	18	γ	5
R_{12}	65	θ_{12}	29		
R: radius in mm, θ: mechanical degree					

Table 2 Magnetic and mechanical features of the studied MCMG machine.

Parameter/symbol	Unit	Value/Name
B_r	T	1.2
PM material	-	NdFeB-N35
Lamination material	-	M19-0.5
Wire material	-	Cu
Number of conductors per slot		20
Rated speed (High speed rotor)	RPM	2100
CVT gear ratio		6, 7/6

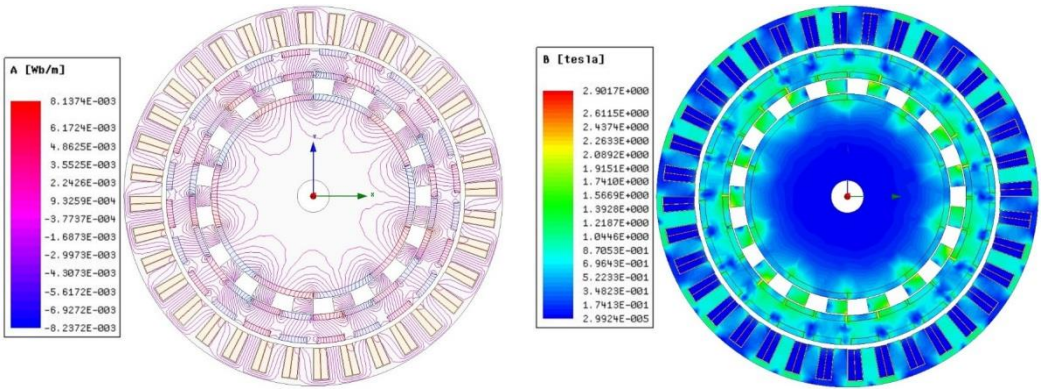

(a) (b)

Fig. 4 Magnetic vector potential (a) and Magnetic flux density distribution in the MCMG machine.

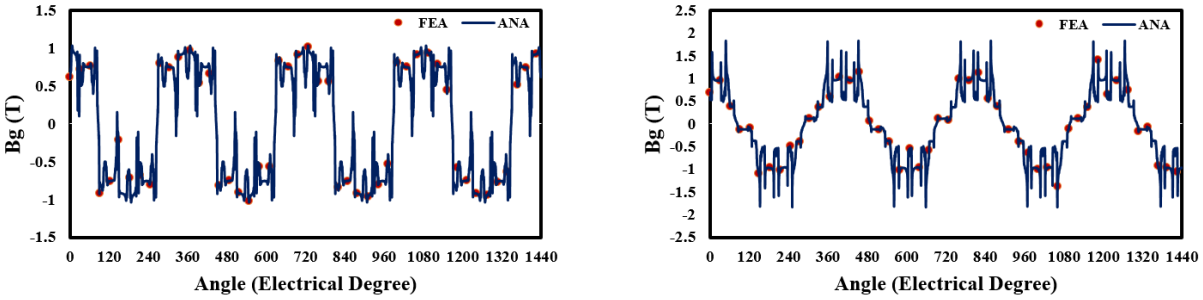

(a) inner air-gap (b) outer air-gap

Fig. 5 An Analytical and finite element analysis of magnetic flux density in, (a) inner air-gap, (b) outer air-gap of the machine.

In this research, in order to evaluate the performance of MCMG machine, three working modes including pure magnetic mode, hybrid mode and charging mode are considered. In pure magnetic mode, it drives the external rotor or shaft modulator. Depending on the choice of each one, the gear ratio will be different, and it is necessary to determine the appropriate gear ratio depending on the loading conditions. If the modulator is stationary, the inner rotor rotates the outer rotor at a ratio of 6 to 1. Fig. 7(a) shows the torque waveform of this situation. In the situation where the inner rotor is considered stationary, the ratio of the rotation of the outer rotor to the modulator will be 6 to 7. In this case, the corresponding torque waveform will be according to Fig. 7 (b). This gear ratio is suitable for driving the car. In Table 3, the electromagnetic torque and ripple torque of the MCMG machine are compared in this working mode.

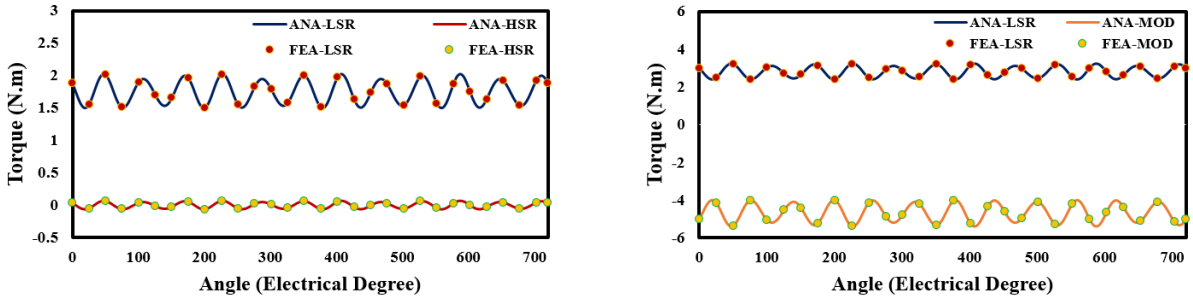

(a) Gr=6 (b) Gr=7/6

Fig. 7 Torque comparison for the MCMG machine at first mode.

Table 3 Magnetic torque/torque ripple comparison at first mode.

Outer rotor steady state torque, N.m		Outer rotor Ripple		Inner rotor steady state torque, N.m		Inner rotor ripple	
Gr1=6	Gr2=7/6	Gr1=6	Gr3=7/6	Gr1=6	Gr2=7/6	Gr1=6	Gr2=7/6
2.35	-6.38	0.782	2.4	0.00042	3.5	0.22	0.543

In the second mode, i.e. the hybrid mode, the coil embedded in the stator can be fed and, in this way, the speed/torque regime of the modulator can be determined by selecting the gear ratio. This mode is especially important when starting the car, which needs to overcome the car's inertia.

In the third mode, i.e. the charging mode, the external rotor and modulator are stationary, and the stator acts as a generator and the electrical energy is stored in the battery. In Table 4, the voltage values of the stored power in the battery are listed assuming that the internal rotor speed is 2100 rpm. The high voltage mode occurs when the modulator and the internal rotor rotate in the same direction with a speed of 300 and 2100 rpm, respectively.

Table 4 A comparison between induced voltages of the studied MCMG machine at third mode.

Induced voltage, V	
Low voltage mode	High voltage mode
8.74	12.42

In order to validate the results of analytical modeling and numerical study, a prototype of MCMG machine has been built and its performance in different working modes has been evaluated by performing experimental tests. The material of the sections and the geometric dimensions are listed in the table below.

Table 5 Parts material and their dimensions

Hybrid low-speed rotor			High-Speed Rotor		
Part Name	Material	Dimension	Part Name	Material	Dimension
Lamination	M-19	0.5mm	Lamination	M19	0.5mm
PM	NdFeB -radial		PM	NdFeB -radial	
Caps	Al	3mm	Shaft	MO-45	L=164mm
Wire	Cu	1mm*20			D=20mm
The effective length of the rotor: 20 mm					

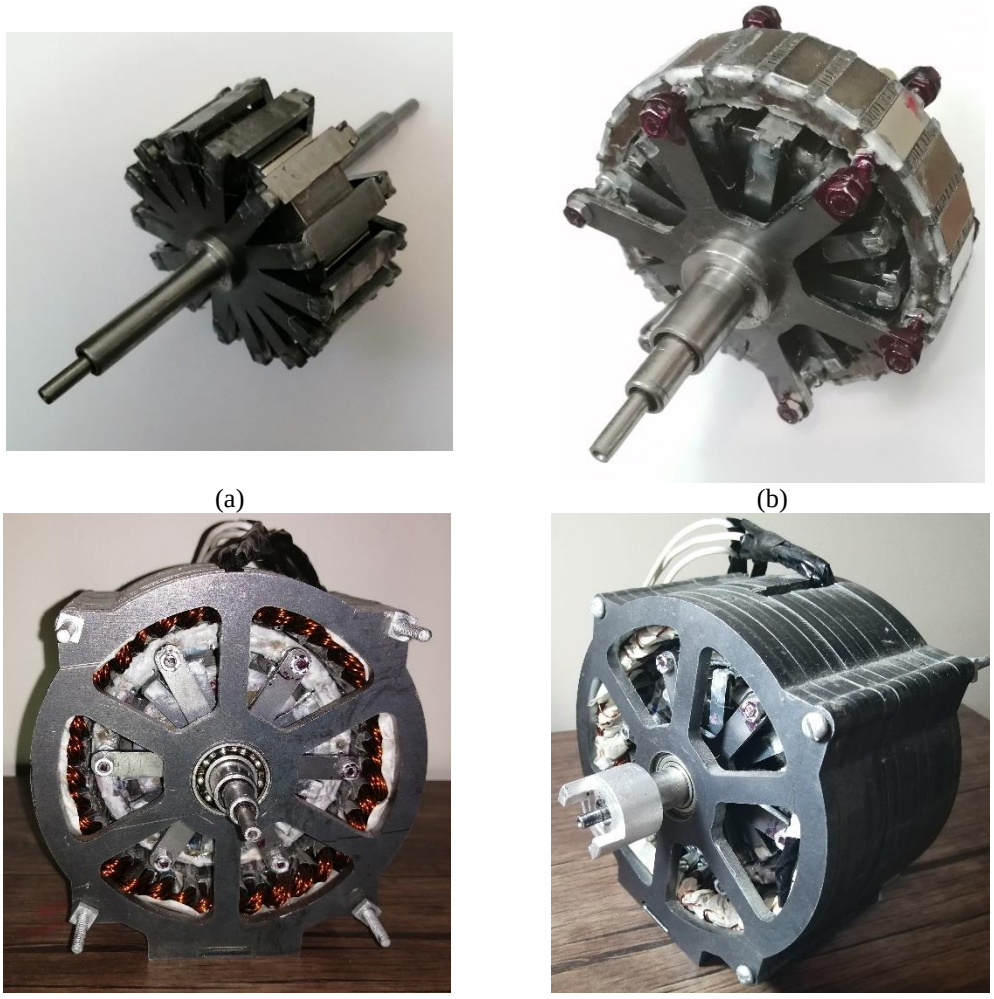

Fig. 8 The MCMG machine, (a) internal rotor and modulator, (b) exiernal rotor (c) the final machine.

Figures 9 to 11 show the MCMG machine coupled with a motor and a generator. How to connect the motor to the power supply and the oscilloscope is also shown. The speed of the motor connected to the machine is 2100 rpm and at any gear ratio an optical sensor reports the rotational speed of the machine.

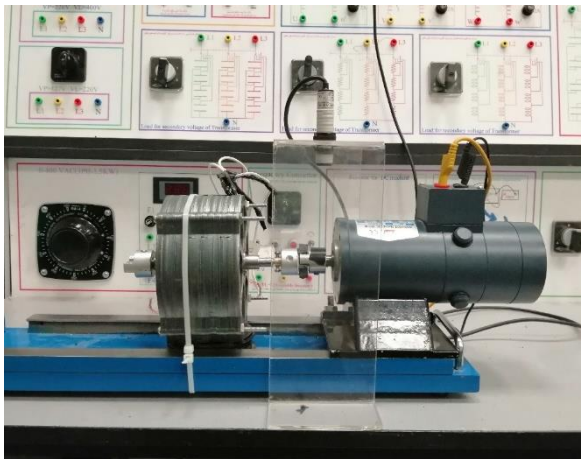

Fig. 9 No-load experimental test of the fabricated CVT gearbox.

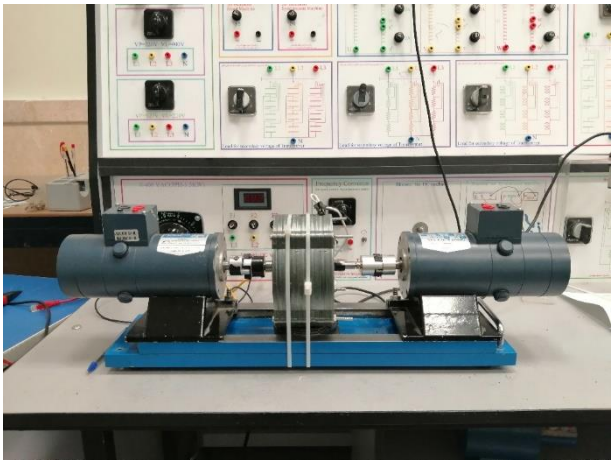

Fig. 10 On-load experimental test of the fabricated CVT gearbox.

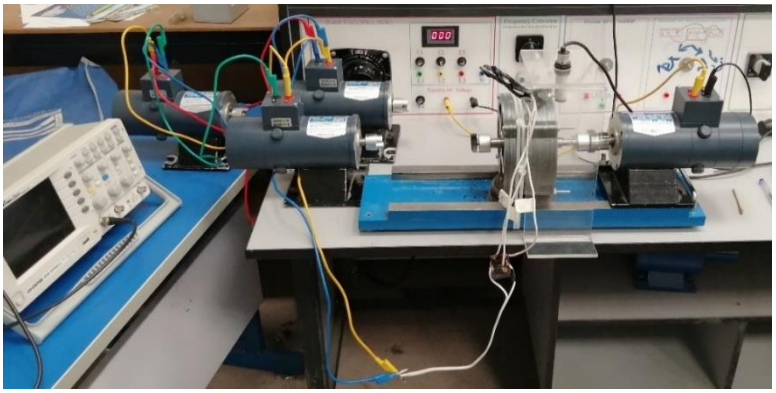

Fig. 11 Generator mode test.

The generator output voltage values in low voltage and high voltage modes are shown in Figures 12(a) and 12(b). These results have been compared at a speed of 2100 rpm. The maximum error percentage is about 3. This difference is not visually recognizable in waveforms shown in Fig.12.

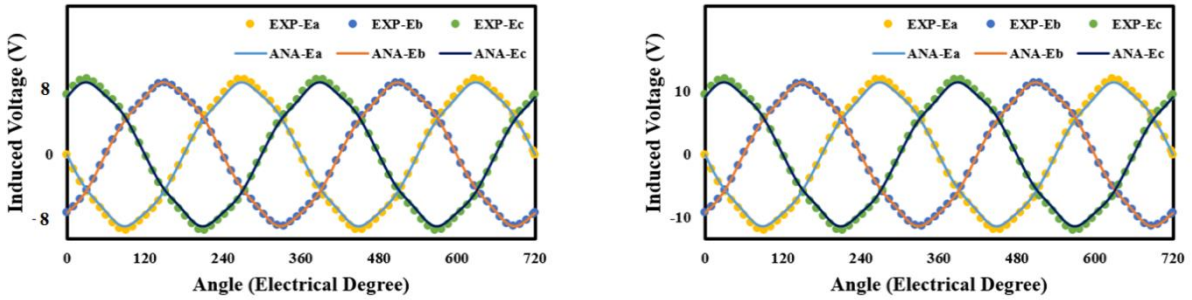

(a) low voltage mode (b) high voltage mode

Fig. 12 Induced voltage comparison for the fabricated MCMG machine at charging mode.

4 Conclusion

In this research, an MCMG machine has been introduced for use in an electric vehicle. The mentioned machine provides the possibility of working in three distinct working modes. To estimate the performance of the machine, an analytical model based on the subdomain method is presented. To validate and evaluate the accuracy of the proposed method, the performance of the machine has been calculated numerically using the finite element analysis method and compared with the analytical method. Also, a machine prototype has been built and experimental tests have been done in three working modes. The comparison of the results shows that the proposed analysis method is highly accurate in estimating the machine's performance and the maximum error percentage is 3%.

Appendix A

Table A1 Magnetic vector potential for inner rotor subdomains.

Region/Limits	General solution
i-th PM region $\Omega = 1$ $t \in [t_3.\, t_4]$ $\theta \in [\theta_1.\, \theta_2]$ $M_{rn} = \frac{4B_r}{\mu_0 n\pi} Sin(\frac{n\pi\alpha_p}{2})$	$A_{z\Omega(k)}(t.\theta) = \sum_{n=1}^{\infty} \left(\frac{{a_n}^{\Omega(k)}(\theta_2 - \theta_1)}{n\pi} \frac{Ch\left(n\pi\left(\frac{t-t_4}{\theta_8-\theta_7}\right)\right)}{Sh\left(n\pi\left(\frac{t_3-t_4}{\theta_8-\theta_7}\right)\right)} + X_n(t) Sin\left(\frac{n\pi\alpha_p}{2\alpha_r}\right) \right) Cos\left(n\pi\left(\frac{\theta-\theta_1}{\theta_2-\theta_1}\right)\right) + \sum_{n=1}^{\infty} \left(\frac{{a_n}^{\Omega(k)}(\theta_2 - \theta_1)}{n\pi} \frac{Ch\left(n\pi\left(\frac{t-t_4}{\theta_8-\theta_7}\right)\right)}{Sh\left(n\pi\left(\frac{t_3-t_4}{\theta_8-\theta_7}\right)\right)} + X_n(t) Sin\left(\frac{n\pi\alpha_p}{2\alpha_r}\right) \right) Sin\left(n\pi\left(\frac{\theta-\theta_1}{\theta_2-\theta_1}\right)\right)$
$X_n(t) = \left(1 + \frac{1}{n} e^{(n+1)t}\right) f_n(t) - \frac{\mathrm{Cosh}\,(n(t-t_4))}{\mathrm{Cosh}\,(n(t_3-t_4))} \left(1 + \frac{1}{n} e^{(n+1)t_3}\right) f_n(t_3)$ $f_n(t) = \begin{cases} \mu_0 \frac{npM_{rn}}{1-np^2} R_2 e^{-t} & if\ np \neq 1 \\ -\mu_0 \frac{M_{rn}}{2} R_2 e^{-t} ln\,(R_2 e^{-t}) & if\ np = 1 \end{cases}$	

Table A2 Magnetic vector potential for modulator subdomain.

Region/Limits	General solution	$f(t)$
j-th modulator slot $\Omega = 4$ $t \in [t_9.\, t_{10}]$ $\theta \in [\theta_5.\, \theta_6]$	$A_{z\Omega(j)}(t.\theta) = {a_0}^{\Omega(j)} + {b_0}^{\Omega(j)} t - f_{\Omega(j)}(t) + \sum_{h=1}^{\infty} \left(\frac{{a_h}^{\Omega(j)}(\theta_6 - \theta_5)}{h\pi} \frac{Sh\left(h\pi\left(\frac{t-t_{10}}{\theta_6-\theta_5}\right)\right)}{Sh\left(h\pi\left(\frac{t_9-t_{10}}{\theta_6-\theta_5}\right)\right)} + \frac{{b_h}^{\Omega(j)}(\theta_6 - \theta_5)}{h\pi} \frac{Sh\left(h\pi\left(\frac{t-t_9}{\theta_6-\theta_5}\right)\right)}{Sh\left(h\pi\left(\frac{t_{10}-t_9}{\theta_6-\theta_5}\right)\right)} \right) Cos\left(h\pi\left(\frac{\theta-\theta_5}{\theta_6-\theta_5}\right)\right)$	0

Table A3 Magnetic vector potential for outer rotor subdomain.

Region/Limits	General solution
k-th PM region $\Omega = 6$ $t \in [t_{13}.\, t_{14}]$ $\theta \in [\theta_7.\, \theta_8]$ $M_{rn} = \frac{4B_r}{\mu_0 n\pi} Sin(\frac{n\pi\alpha_p}{2})$	$A_{z\Omega(k)}(t.\theta) = \sum_{n=1}^{\infty} \left(\frac{{a_n}^{\Omega(k)}(\theta_8 - \theta_7)}{n\pi} \frac{Ch\left(n\pi\left(\frac{t-t_{14}}{\theta_8-\theta_7}\right)\right)}{Sh\left(n\pi\left(\frac{t_{13}-t_{14}}{\theta_8-\theta_7}\right)\right)} + X_n(t) Sin\left(\frac{n\pi\alpha_p}{2\alpha_r}\right) \right) Cos\left(n\pi\left(\frac{\theta-\theta_7}{\theta_8-\theta_7}\right)\right)$

	$+\sum_{n=1}^{\infty}\left(\begin{array}{c}\frac{{a_n}^{\Omega(k)}(\theta_8-\theta_7)}{n\pi}\frac{Ch\left(n\pi\left(\frac{t-t_{14}}{\theta_8-\theta_7}\right)\right)}{Sh\left(n\pi\left(\frac{t_{13}-t_{14}}{\theta_8-\theta_7}\right)\right)}\\ +X_n(t)Sin\left(\frac{n\pi\alpha_p}{2\alpha_r}\right)\end{array}\right)Sin\left(n\pi\left(\frac{\theta-\theta_7}{\theta_8-\theta_7}\right)\right)$
$X_n(t)=\left(1+\frac{1}{n}e^{(n+1)t}\right)f_n(t)-\frac{\mathrm{Cosh}\,(n(t-t_{14}))}{\mathrm{Cosh}\,(n(t_{13}-t_{14}))}\left(1+\frac{1}{n}e^{(n+1)t_{13}}\right)f_n(t_{13})$ $f_n(t)=\begin{cases}\mu_0\frac{npM_{rn}}{1-np^2}R_6e^{-t} & if\ np\neq 1\\ -\mu_0\frac{M_{rn}}{2}R_6e^{-t}ln\,(R_6e^{-t}) & if\ np=1\end{cases}$	
k-th PM region $\Omega=7$ $t\in[t_{15}.t_{16}]$ $\theta\in[\theta_{10}.\theta_{11}]$ $M_{rn}=\frac{4B_r}{\mu_0 n\pi}Sin(\frac{n\pi\alpha_p}{2})$	$A_{z\Omega(k)}(t.\theta)=\sum_{n=1}^{\infty}\left(\begin{array}{c}\frac{{a_n}^{\Omega(k)}(\theta_{11}-\theta_{10})}{n\pi}\frac{Ch\left(n\pi\left(\frac{t-t_{16}}{\theta_{11}-\theta_{10}}\right)\right)}{Sh\left(n\pi\left(\frac{t_{15}-t_{16}}{\theta_{11}-\theta_{10}}\right)\right)}\\ +X_n(t)Sin\left(\frac{n\pi\alpha_p}{2\alpha_r}\right)\end{array}\right)Cos\left(n\pi\left(\frac{\theta-\theta_{10}}{\theta_{11}-\theta_{10}}\right)\right)$ $+\sum_{n=1}^{\infty}\left(\begin{array}{c}\frac{{a_n}^{\Omega(k)}(\theta_{11}-\theta_{10})}{n\pi}\frac{Ch\left(n\pi\left(\frac{t-t_{16}}{\theta_{11}-\theta_{10}}\right)\right)}{Sh\left(n\pi\left(\frac{t_{15}-t_{16}}{\theta_{11}-\theta_{10}}\right)\right)}\\ +X_n(t)Sin\left(\frac{n\pi\alpha_p}{2\alpha_r}\right)\end{array}\right)Sin\left(n\pi\left(\frac{\theta-\theta_{10}}{\theta_{11}-\theta_{10}}\right)\right)$
$X_n(t)=\left(1+\frac{1}{n}e^{(n+1)t}\right)f_n(t)-\frac{\mathrm{Cosh}\,(n(t-t_{11}))}{\mathrm{Cosh}\,(n(t_{10}-t_{11}))}\left(1+\frac{1}{n}e^{(n+1)t_{10}}\right)f_n(t_{10})$ $f_n(t)=\begin{cases}\mu_0\frac{npM_{rn}}{1-np^2}R_8e^{-t} & if\ np\neq 1\\ -\mu_0\frac{M_{rn}}{2}R_8e^{-t}ln\,(R_8e^{-t}) & if\ np=1\end{cases}$	

Table A4 Magnetic vector potential for stator subdomain.

Region/Limits	General solution	$f(t)$
m-th stator slot $\Omega=9$ $t\in[t_{21}.t_{22}]$ $\theta\in[\theta_{13}.\theta_{14}]$	$A_{z\Omega(m)}(t.\theta)={a_0}^{\Omega(m)}-f_{z\Omega(m)}(t)$ $+\sum_{h=1}^{\infty}\frac{{a_h}^{\Omega(l)}(\theta_{14}-\theta_{13})}{4h\pi}\frac{Ch\left(4h\pi\left(\frac{t-t_{22}}{\theta_{14}-\theta_{13}}\right)\right)}{Sh\left(4h\pi\left(\frac{t_{21}-t_{22}}{\theta_{14}-\theta_{13}}\right)\right)}Cos\left(4h\pi\left(\frac{\theta-\theta_{13}}{\theta_{14}-\theta_{13}}\right)\right)$	$-\frac{1}{2}\mu_0 J_i\left(e^{-t_{21}t}+\frac{1}{2}e^{-2t+t_{21}}\right)$

Table A5 Magnetic for all periodic air-gap subdomains.

Region/Limits	General solution
First air-gap $\Omega=3$ $t\in[t_5.t_6]$ $\theta\in[0.2\pi]$	$A_{z\Omega}(\mathrm{t}.\theta)=\sum_{n=1}^{\infty}\frac{1}{n}\left(\begin{array}{c}{a_n}^{\Omega}\frac{Ch(n(\mathrm{t}-t_6))}{Sh(n(t_5-t_6))}\\ +{b_n}^{\Omega}\frac{Ch(n(\mathrm{t}-t_5))}{Sh(n(t_6-t_5))}\end{array}\right)Cos(n\theta)+\sum_{n=1}^{\infty}\frac{1}{n}\left(\begin{array}{c}{c_n}^{\Omega}\frac{Ch(n(\mathrm{t}-t_6))}{Sh(n(t_5-t_6))}\\ +{d_n}^{\Omega}\frac{Ch(n(\mathrm{t}-t_5))}{Sh(n(t_6-t_5))}\end{array}\right)Sin(n\theta)$
Second air-gap $\Omega=5$ $t\in[t_{11}.t_{12}]$ $\theta\in[0.2\pi]$	$A_{z\Omega}(\mathrm{t}.\theta)=\sum_{n=1}^{\infty}\frac{1}{n}\left(\begin{array}{c}{a_n}^{\Omega}\frac{Ch(n(\mathrm{t}-\mathrm{t}_{12}))}{Sh\left(n(\mathrm{t}_{t_{11}}-\mathrm{t}_{12})\right)}\\ +{b_n}^{\Omega}\frac{Ch(n(\mathrm{t}-t_{11}))}{Sh(n(\mathrm{t}_{12}-t_{11}))}\end{array}\right)Cos(n\theta)+\sum_{n=1}^{\infty}\frac{1}{n}\left(\begin{array}{c}{c_n}^{\Omega}\frac{Ch(n(\mathrm{t}-\mathrm{t}_{12}))}{Sh(n(t_{11}-\mathrm{t}_{12}))}\\ +{d_n}^{\Omega}\frac{Ch(n(\mathrm{t}-t_{11}))}{Sh(n(\mathrm{t}_{12}-t_{11}))}\end{array}\right)Sin(n\theta)$

Third air-gap $\Omega = 8$ $t \in [t_{19}.t_{20}]$ $\theta \in [0.2\pi]$	$A_{z\Omega}(\mathrm{t}.\theta) = \sum_{n=1}^{\infty}\frac{1}{n}\left(\begin{matrix}{a_n}^{\Omega}\frac{Ch(n(\mathrm{t}-\mathrm{t}_{20}))}{Sh(n(\mathrm{t}_{19}-\mathrm{t}_{20}))}\\ +{b_n}^{\Omega}\frac{Ch(n(\mathrm{t}-\mathrm{t}_{19}))}{Sh(n(\mathrm{t}_{20}-\mathrm{t}_{19}))}\end{matrix}\right)Cos(n\theta) + \sum_{n=1}^{\infty}\frac{1}{n}\left(\begin{matrix}{c_n}^{\Omega}\frac{Ch(n(\mathrm{t}-\mathrm{t}_{20}))}{Sh(n(\mathrm{t}_{19}-\mathrm{t}_{20}))}\\ +{d_n}^{\Omega}\frac{Ch(n(\mathrm{t}-\mathrm{t}_{19}))}{Sh(n(\mathrm{t}_{20}-\mathrm{t}_{19}))}\end{matrix}\right)Sin(n\theta)$

Table 6A θ-axis conditions

$\boldsymbol{r = R_3}$		$\boldsymbol{r = R_4}$	
$A_{z3(i)}\big\vert_{t=t_4} = A_{z5}\vert_{t=t_5}$	$\forall\theta \in [\theta_1.\theta_2]$	$A_{z5)}\big\vert_{t=t_6} = A_{z7(j)}\big\vert_{t=t_7}$	$\forall\theta \in [\theta_5.\theta_6]$
$D_{\theta3(i)}\big\vert_{t=t_4} = D_{\theta5}\vert_{t=t_5}$	$\forall\theta \in [\theta_1.\theta_2]$	$D_{\theta5)}\big\vert_{t=t_6} = D_{\theta7(j)}\big\vert_{t=t_7}$	$\forall\theta \in [\theta_5.\theta_6]$
$A_{z4(i)}\big\vert_{t=t_4} = A_{z5}\vert_{t=t_5}$	$\forall\theta \in [\theta_2.\theta_3]$	$\boldsymbol{r = R_5}$	
$D_{\theta4(i)}\big\vert_{t=t_4} = D_{\theta5}\vert_{t=t_5}$	$\forall\theta \in [\theta_2.\theta_3]$	$A_{z7(j)}\big\vert_{t=t_8} = A_{z8}\vert_{t=t_9}$	$\forall\theta \in [\theta_5.\theta_6]$
		$D_{\theta7(j)}\big\vert_{t=t_8} = D_{\theta8}\vert_{t=t_9}$	$\forall\theta \in [\theta_5.\theta_6]$
$\boldsymbol{r = R_6}$		$\boldsymbol{r = R_7}$	
$A_{z8}\vert_{t=t_{10}} = A_{z9(k)}\big\vert_{t=t_{11}}$	$\forall\theta \in [\theta_7.\theta_8]$	$A_{z12(k)}\big\vert_{t=t_{16}} = A_{z14}\vert_{t=t_{17}}$	$\forall\theta \in [\theta_{10}.\theta_{11}]$
$D_{\theta8}\vert_{t=t_{10}} = D_{\theta9(k)}\big\vert_{t=t_{11}}$	$\forall\theta \in [\theta_7.\theta_8]$	$D_{\theta12(k)}\big\vert_{t=t_{16}} = D_{\theta14}\vert_{t=t_{17}}$	$\forall\theta \in [\theta_{10}.\theta_{11}]$
$\boldsymbol{r = R_{10}}$			
$A_{z14}\vert_{t=t_{18}} = A_{z15(m)}\big\vert_{t=t_{19}}$		$\forall\theta \in [\theta_{13}.\theta_{14}]$	
$D_{\theta14}\vert_{t=t_{18}} = D_{\theta15(m)}\big\vert_{t=t_{19}}$		$\forall\theta \in [\theta_{13}.\theta_{14}]$	

Appendix B

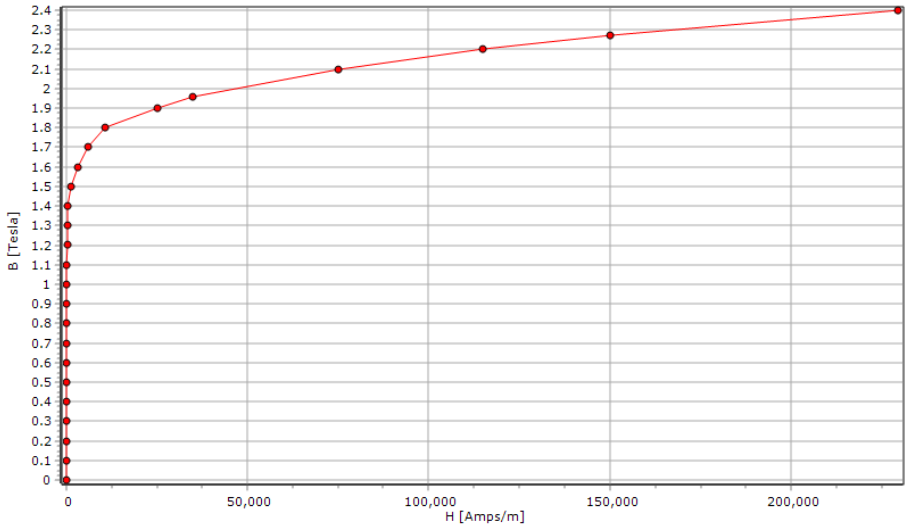

Fig. B1 The B-H curve of the core laminations.

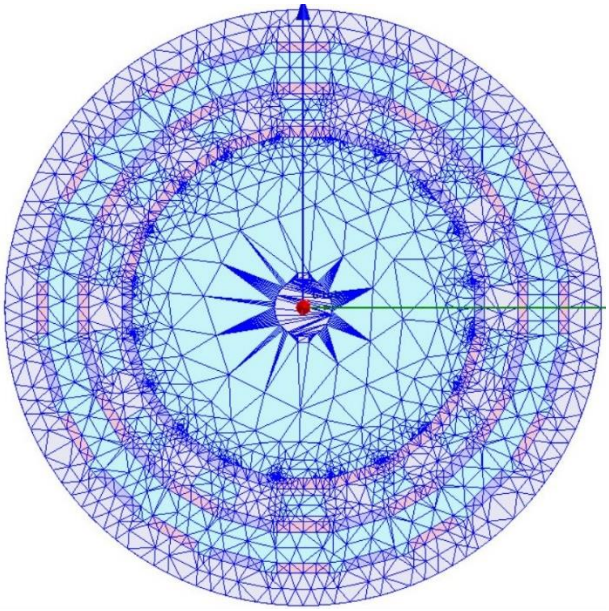

Fig. B2 The mesh density of the investigated MCMG machine.

Reference

1. El-Refaie, Ayman M. "Fractional-slot concentrated-windings synchronous permanent magnet machines: Opportunities and challenges." *IEEE Transactions on industrial Electronics* 57, no. 1 (2009): 107-121.
2. Zhu, Zi-Qiang, and David Howe. "Electrical machines and drives for electric, hybrid, and fuel cell vehicles." *Proceedings of the IEEE* 95, no. 4 (2007): 746-765.
3. Levi, Emil. "Multiphase electric machines for variable-speed applications." *IEEE Transactions on industrial electronics* 55, no. 5 (2008): 1893-1909.
4. Atallah, Kais, Jan Rens, Smail Mezani, and David Howe. "A novel "pseudo" direct-drive brushless permanent magnet machine." *IEEE transactions on magnetics* 44, no. 11 (2008): 4349-4352.
5. Chau, K. T., Dong Zhang, J. Z. Jiang, Chunhua Liu, and Yuejin Zhang. "Design of a magnetic-geared outer-rotor permanent-magnet brushless motor for electric vehicles." *IEEE transactions on magnetics* 43, no. 6 (2007): 2504-2506.
6. Wang, L. L., J. X. Shen, Y. Wang, and K. Wang. "A novel magnetic-geared outer-rotor permanent-magnet brushless motor." (2008): 33-36.
7. Atallah, Kais, Jan Rens, Smail Mezani, and David Howe. "A novel "pseudo" direct-drive brushless permanent magnet machine." *IEEE transactions on magnetics* 44, no. 11 (2008): 4349-4352.
8. Tlali, P. M., R. J. Wang, and S. Gerber. "Magnetic gear technologies: A review." In *2014 International Conference on Electrical Machines (ICEM)*, pp. 544-550. IEEE, 2014.
9. Atallah, Kais, and David Howe. "A novel high-performance magnetic gear." *IEEE Transactions on magnetics* 37, no. 4 (2001): 2844-2846.
10. Tsurumoto, K., and S. Kikuchi. "A new magnetic gear using permanent magnet." *IEEE Transactions on Magnetics* 23, no. 5 (1987): 3622-3624.
11. McGilton, Ben, Richard Crozier, Alasdair McDonald, and Markus Mueller. "Review of magnetic gear technologies and their applications in marine energy." *IET Renewable Power Generation* 12, no. 2 (2018): 174-181.
12. Gerber, S., and R. J. Wang. "Evaluation of a prototype magnetic gear." In *2013 IEEE International Conference on Industrial Technology (ICIT)*, pp. 319-324. IEEE, 2013.
13. Praslicka, Bryton, Matthew C. Gardner, Matthew Johnson, and Hamid A. Toliyat. "Review and analysis of coaxial magnetic gear pole pair count selection effects." *IEEE Journal of Emerging and Selected Topics in Power Electronics* 10, no. 2 (2021): 1813-1822.
14. Jian, Linni, and K. T. Chau. "A coaxial magnetic gear with Halbach permanent-magnet arrays." *IEEE Transactions on Energy conversion* 25, no. 2 (2010): 319-328.
15. Filippini, Mattia, and Piergiorgio Alotto. "Coaxial magnetic gear design and optimization." *IEEE Transactions on Industrial Electronics* 64, no. 12 (2017): 9934-9942.
16. Jing, Libing, Lin Liu, Min Xiong, and Da Feng. "Parameters analysis and optimization design for a concentric magnetic gear based on sinusoidal magnetizations." *IEEE Transactions on Applied superconductivity* 24, no. 5 (2014): 1-5.
17. Xu, Longya. "A new breed of electric machines-basic analysis and applications of dual mechanical port electric machines." In *2005 International Conference on Electrical Machines and Systems*, vol. 1, pp. 24-31. IEEE, 2005.
18. Cheng, Ming, Peng Han, Giuseppe Buja, and Milutin G. Jovanović. "Emerging multiport electrical machines and systems: Past developments, current challenges, and future prospects." *IEEE Transactions on Industrial electronics* 65, no. 7 (2017): 5422-5435.
19. Zhu, Z. Q., and D. Evans. "Overview of recent advances in innovative electrical machines—With particular reference to magnetically geared switched flux machines." In *2014 17th International Conference on Electrical Machines and Systems (ICEMS)*, pp. 1-10. IEEE, 2014.
20. Fu, W. N., and Yulong Liu. "A unified theory of flux-modulated electric machines." In *2016 International Symposium on Electrical Engineering (ISEE)*, pp. 1-13. IEEE, 2016.
21. Jabbari, Ali, and A. Baderan. "Segmented Hybrid-PM Machines for Electric Vehicles; Semi-Analytical, Numerical and Experimental Study." *Iranian Journal of Electrical & Electronic Engineering* 19, no. 3 (2023).
22. Tavakoli, Gholamreza, Ali Jabbari, and Mohammad Reza Sheykholeslami. "A semi-analytical, numerical and experimental study on performance characteristics of a novel hybrid-rotor CVT magnetic gearbox." *Proceedings of the Institution of Mechanical Engineers, Part D: Journal of Automobile Engineering* 237, no. 8 (2023): 1994-2005.
23. Jabbari, A. "The Effect of Dummy Slots on Machine Performance in Brushless Permanent Magnet Machines: An Analytical, Numerical, and Experimental Study." *Iranian Journal of Electrical & Electronic Engineering* 18, no. 2 (2022).
24. Jabbari, Ali, and Frédéric Dubas. "The Effect of Magnet Width and Iron Core Relative Permeability on Iron Pole Radii Ratio in Spoke-Type Permanent-Magnet Machine: An Analytical, Numerical and Experimental Study." *Iranian Journal of Electrical and Electronic Engineering* 17, no. 2 (2021): 1802-1802.
25. Jabbari, Ali, and Frédéric Dubas. "An improved model for performances calculation in spoke-type permanent-magnet machines considering magnetization orientation and finite soft-magnetic material permeability." *COMPEL-The international journal for computation and mathematics in electrical and electronic engineering* 39, no. 6 (2020): 1299-1314.
26. Jabbari, Ali, Hosein Taheri, and Ali Asghar Ghadimi. "An analytical, numerical and experimental study on performance characteristics in a novel Vernier permanent magnet machine." *Electrical Engineering* 102 (2020): 2369-2379.
27. Jabbari, Ali, and Frédéric Dubas. "Analytical Modelling of Magnetic Field Distribution in Spoke Type Permanent Magnet Machines." *Journal of Iranian Association of Electrical and Electronics Engineers* 17, no. 3 (2020): 141-151.
28. Jabbari, A. "Analytical modeling of magnetic field distribution in multiphase H-type stator core permanent magnet flux switching machines." *Iranian Journal of Science and Technology, Transactions of Electrical Engineering* 43, no. Suppl 1 (2019): 389-401.
29. Jabbari, Ali. "An analytical study on iron pole shape optimization in high-speed interior permanent magnet machines." *Iranian Journal of Science and Technology, Transactions of Electrical Engineering* 44, no. 1 (2020): 169-174.
30. Jabbari, Ali. "An analytical expression for magnet shape optimization in surface-mounted permanent magnet machines." *Mathematical and Computational Applications* 23, no. 4 (2018): 57.
31. Jabbari, A. "Analytical modeling of magnetic field distribution in inner rotor brushless magnet segmented surface inset permanent magnet machines." *Iranian Journal of Electrical and Electronic Engineering* 14, no. 3 (2018): 259-269.
32. Jabbari, Ali. "Exact analytical modeling of magnetic vector potential in surface inset permanent magnet DC

machines considering magnet segmentation." *Journal of Electrical Engineering* 69, no. 1 (2018): 39-45.\
33. Jabbari, A. "2D analytical modeling of magnetic vector potential in surface mounted and surface inset permanent magnet machines." *Iranian Journal of Electrical and Electronic Engineering* 13, no. 4 (2017): 362-373.
34. Jabbari, Ali. "Design optimization of a permanent magnet brushless generator for a gearless wind turbine." In *2016 Iranian Conference on Renewable Energy & Distributed Generation (ICREDG)*, pp. 56-62. IEEE, 2016.\
35. Jabbari, A., M. Shakeri, and A. Nabavi. "Shape optimization of permanent magnet motors using the reduced basis technique." *World Academy of Science, Engineering and Technology* 49 (2009): 592-597.
36. Jabbari A. "Semi-Analytical Modeling of Electromagnetic Performances in Magnet Segmented Spoke-Type Permanent Magnet Machine Considering Infinite and Finite Soft-Magnetic Material Permeability." *Iranian Journal of Electrical & Electronic Engineering*. 17, no 1 (2021): 1-13
37. Jabbari A, Dubas F. "A New Subdomain Method for Performances Computation in Interior Permanent-Magnet (IPM) Machines." *Iranian Journal of Electrical & Electronic Engineering*. 16, no 1 (2020): 26-38.
38. Jabbari, A., Shakeri, M. and Niaki, S.N. "Pole shape optimization of permanent magnet synchronous motors using the reduced basis technique." *Iranian Journal of Electrical and Electronic Engineering*, 6 no 2 (2010): 48-55.
39. Jabbari, A., Shakeri, M. and Gholamian, A.S. "Rotor pole shape optimization of permanent magnet brushless DC motors using the reduced basis technique". *Advances in electrical and computer engineering*, 9 no 2(2009): 75-81. 75-81.
40. Jabbari, A., Shakeri, M. and Nabavi, N.S., "Torque ripple minimization in PM synchronous motors using tooth shape optimization." (2010). 27-31

Jabbari, A., Shakeri, M. and Niaki, A.N. "Iron pole shape optimization of IPM Motors using an Integrated Method". *Advances in Electrical and Computer Engineering Journal*, 10, no 2(2010): 67-70.

Ali Jabbari was born in Shazand, Iran, in 1980. He received the B.Sc degree from the "Iran University of Science and Technology" in 2002 and his M.Sc. and Ph.D. degrees both in Manufacturing and Production Engineering from "Mazandran University" in 2004 and 2009, respectively, with a focus on the design and optimization of Brushless DC permanent magnet machines for direct drive applications.
He is currently an Associate Professor with the Department of Manufacturing and Production Engineering, at Arak University, Arak, Iran. Since 2014, he has been the Head of the "Gearless Wind Turbine Project" team.
Interests: Gearless Wind Turbine Design, Analytical Modeling, PM Machines, Subdomain Technique, Friction Stir Welding, Metal Forming.

Hassan Moradzadeh was born in Holy Mashhad, in 1972. He received his B.Sc., M.Sc., and PhD degrees in Electrical Engineering and Electronics from Amir Kabir, Guilan and Iran University of Science and Technology (IUST) Universities, respectively. He has experienced about ten years of work with domestic corporations in telecommunication and switching eras as a HW/SW and R&D designer. He has been with Arak University since about 2011 as an Assistant Professor, teaching in Electronics and Mechatronics fields. His current research interests include Embedded Systems Design, Mechatronic Systems Implementation, and Artificial Intelligence.

Rasoul Lotfi was born in NajafAbab, Iran, in 1987. He received the B.Sc degree in Mechanical Engineering from the "Islamic Azad University of Takestan" in 2011 and his MSc degrees in Mechanical Engineering - mechatronic from "Arak University" in 2019 respectively, with a search and development on "magnetic gears".
He is currently working as a mechanical engineer at Iranab Consulting Engineers, Tehran, Iran in WWTP & WTP.
Interests: concentric magnetic gearboxes, renewable energies, energy optimization, incompressible turbo machines, environment.
More info: https://www.linkedin.com/in/rasoul-lotfi-44642172/